Korean J. Chem. Eng., 32(12), 2542-2549 (2015)
DOI: 10.1007/s11814-015-0157-0

pISSN: 0256-1115
eISSN: 1975-7220

Effects of angle on the transport velocity in an inclined fluidized-bed

Muhammad Shahzad Khurram*, Jeong-Hoo Choi*,†, Yoo Sube Won*, A Reum Jeong*, Young Cheol Park, Ho-Jung Ryu**, and Chang-Keun Yi****

*Department of Chemical Engineering, Konkuk University, 1 Hwayang-dong, Gwangjin-gu, Seoul 143-701, Korea
**Korea Institute of Energy Research, 71-2, Jang-dong, Yuseong-gu, Daejeon 305-343, Korea
(*Received 5 February 2015 • accepted 20 July 2015*)

Abstract−The transport velocity (u_{tri}) in an inclined fluidized-bed was investigated by varying the bed angle relative to the horizontal plane (0^o-90^o), the particle diameter (0.021-0.925 mm), and density (1,272-4,503 kg/m^3). This study employed the emptying time method to determine the transport velocity. The transport velocity for the vertical fluidized-bed (u_{tr90}) was revealed to increase appreciably with the aspect ratio of the fluidized-bed. The transport velocity decreased as the bed angle increased. The ratio of the transport velocity to that for the vertical bed (u_{tri}/u_{tr90}) decreased with an increase in either the bed angle or the ratio of the particle diameter (d_p) to the critical particle diameter (d_p^*), i.e., the maximum particle diameter at which the sum of the interparticle adhesion forces had a dominant influence on particle entrainment. Correlations for the transport velocity according to the bed angle relative to the horizontal plane were proposed successfully, based on the experimental data.

Keywords: Transport Velocity, Correlation, Fluidized-bed, Riser, Inclined Fluidized-bed, Bed Angle

INTRODUCTION

A fluidized-bed inclined relative to the vertical axis can be applied as an inclined standpipe or an inclined riser in a pneumatic conveying system. The multistage fluidized-bed process used for reducing iron ore has an inclined standpipe between two consecutive bubbling fluidized-beds. The standpipe is a simple pipeline without any mechanical and nonmechanical valves in it. The solid reactant descends from the upper reactor to the lower one through the standpipe, and the gas reactant coming out of the cyclone in the lower reactor enters the upper reactor through the plenum and distributor as a fluidizing gas. The inlet of the inclined standpipe is located at the surface level of the upper fluidized-bed and the outlet in the bottom of the lower fluidized-bed. The particles of the upper bed enter the inlet by overflow, and part of the reactant gas entering the outlet from the lower bed ascends the standpipe as a countercurrent to the solids' flow. Under this condition, the gas velocity in the standpipe should be controlled to be lower than the transport velocity of the solids to maintain the solids' seal and eventually keep the process from shutting down by the bypass of the fluidizing gas. Youn and Choi [1] investigated the maximum permissible fluidizing velocity of the lower bed for a standpipe to work safely in a laboratory-scale two-stage bubbling fluidized-bed model at room temperature and pressure and proposed a correlation for it. However, they could not reveal the gas velocity in the standpipe.

Another example of an inclined fluidized-bed is the inclined riser in a pneumatic conveying system. The solid product from the multistage fluidized-bed process for reducing iron ore is sent to the storage from the bottom of the lowest fluidized-bed through an inclined riser. This operation uses a part of the reactant gas in the bed as the conveying gas, and thus the flow rate of this gas should be minimized. Under similar conditions, the inclined riser is used as a part of the pneumatic transport of particles from one reactor to another in fluid catalytic cracking (FCC) and fluid coking processes [2]. In the design of a pneumatic conveying pipeline, which generally consists of horizontal and vertical sections having the same pipe size, the minimum flow rate of the conveying gas is governed by the gas velocity of the horizontal section because the minimum gas velocity required for the horizontal section is usually greater than that for the vertical section. Then, the gas flow rate is excessive to the minimum required rate for the vertical section. One may consider increasing the gas velocity in the horizontal section by employing the diameter of the horizontal section smaller than that of the vertical one at the minimum gas flow rate for the vertical section. However, it results in potential issues such as high pressure drop, solid degradation, or pipe erosion in the line. The minimum gas velocity for the inclined riser lies between the gas velocities for the vertical and the horizontal risers. Therefore, an inclined riser is preferable to reduce the excess gas flow rate and eliminate the abovementioned issues.

However, no basic studies have measured the minimum gas velocity required to transport particles in an inclined fluidized-bed, unlike in the case of a vertical fluidized-bed. In a vertical fluidized-bed, the transport velocity was studied as the transition velocity between the low-velocity fluidization at which most particles stay in the bed and the transport operation of particles [3-17], which refers to the minimum velocity for the transport mode of fluidization. Several correlations for the velocity as a function of the gas and particle properties have also been reported in literature [10,11,14,16,18,19]. The transport velocity increased with either the particle size or the

†To whom correspondence should be addressed.
E-mail: choijhoo@konkuk.ac.kr

particle density; however, it was considered independent of column dimensions such as the diameter and height [20]. Under the precondition that most solids left in the pipeline at accidental shutdown must be cleaned easily by gravity, the angle of the standpipe and riser relative to the horizontal plane should be larger than the repose angle of particles. At this column angle, the resistance against particle transport mainly comes from gravity along with the additional minor effects of interparticle adhesion forces. Then, the minimum transport velocity at the condition (u_{tri}) can be approximated as a property equal to that in the vertical fluidized-bed (u_{tr90}) to apply the same method as that used in the measurement of u_{tr90} for determining u_{tri}.

We investigated the characteristics of the transport velocity in the inclined fluidized-bed. The emptying time method proposed by Han et al. [7] for the vertical fluidized-bed was employed to determine the transport velocity, and the variations of the particle size and density and the angle of the fluidized-bed were considered as experimental variables at ambient temperature and pressure.

EXPERIMENTAL

The experimental setup consisted of a compressor, a mass flow meter controller, a fluidized-bed (inner diameter: 0.05 m, height: 1 m), a bag filter, and a data logger connected to a differential pressure transducer (Fig. 1). The fluidized bed was made of transparent Plexiglas and inclined with an angle to the horizontal plane. Air was used as the fluidizing gas, and its flow rate was set by a mass flow meter controller. A differential pressure transducer was used to measure the axial pressure drop in the fluidized-bed.

The bed materials were ten groups of particles (plastic, spent FCC catalyst, glass beads (GB) of different sizes, sand and iron ore) defined narrowly in size and classified as Geldart's type A, B, and D particles (see Table 1) [21]. The repose angles (θ_r) of the particles were determined according to the fixed funnel method [22]. The repose angle of the glass beads seemed to show a minimum about the mean diameter of 0.167 mm as the particle size increased, as also reported by Kang [23]. Table 1 also shows the terminal velocity calculated by the correlation of Haider and Levenspiel [24], and critical particle diameter (d_p^*), i.e., the maximum particle diameter at which the sum of the interparticle adhesion forces had a dominant influence on particle entrainment [25,26]. The critical particle diameter d_p^* in meters was given by Ma and Kato [25] as

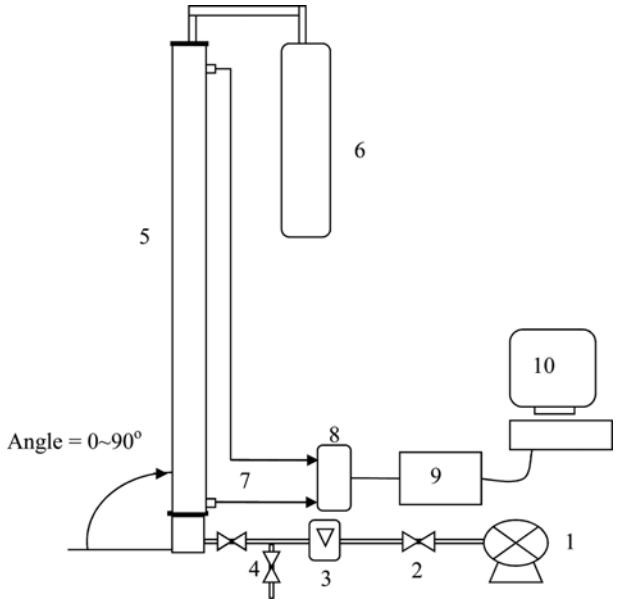

Fig. 1. Experimental set-up.

1. Compressor
2. Valve
3. Flow meter
4. Bypass to bag filter
5. Inclined fluidized-bed
6. Bag filter
7. Pressure taps
8. Pressure transducer
9. Data logger
10. Personal computer

$$d_p^* = 0.101/(g\rho_s^{0.731}) \quad (1)$$

In Eq. (1), g is the gravitational acceleration (9.8 m/s^2) and ρ_s, the apparent particle density in kg/m^3. The mean diameters (d_p) of all particles except GB-21 and plastic were greater than the critical diameter. The transport velocity (u_{tri}) of GB-21 was expected to be

Table 1. Particle properties

Bed angle [degree]	Particles	Specific surface mean diameter (d_p) [μm]	Apparent density [kg/m^3]	Repose angle [degree] [22]	Geldart's Classification [21]	Terminal velocity [m/s] [24]	Critical particle diameter (d_p^*) [μm] [25]
0-90	GB-21	21	2364	29	A	0.03	35.3
	GB-40	40	2440	25	A	0.11	34.4
	GB-167	167	2374	22	B	1.27	35.2
	GB-295	295	2416	24	B	2.27	34.7
	GB-646	646	2418	24	B/D	4.98	34.7
	GB-925	925	2523	24	D	7.33	33.6
	Spent FCC	92	1470	31	A/B	0.38	49.9
	Sand	79	2591	30	A	0.49	33.0
	Iron ore	75	4503	28	B	0.77	22.0
90	Plastic	50	1272	36	A	0.10	55.5

GB: glass bead

appreciably dependent on the interparticle adhesion forces. In fact, the interparticle adhesion forces evidently influenced the flow characteristics of GB-21, GB-40, FCC and sand particles for fluidized-bed angles smaller than the repose angle of the particles.

The transport velocity was determined at ambient temperature and pressure by the emptying time method [7], which measured the time required for transporting all bed particles out of the fluidized-bed at a given gas velocity. The experimental procedure is as follows: (1) initially, place 0.4 kg of particles in the bed; (2) set the rate of gas to flow to the bag-filter through the gas line bypassing the fluidized-bed; (3) switch the gas flow into the fluidized-bed instantaneously to transport the particles out of the bed; and (4) during the series of operations, measure the pressure drop between the bottom of the bed and the gas exit using the pressure transducer.

The fluidizing gas initiated the transport of particles by producing a peak bed pressure drop and finished it when the bed pressure drop leveled off after a decrease to a minimum. Although the peak pressure drop decreased as the angle of the fluidized-bed relative to the horizontal plane decreased, the emptying time method was valid without particle dunes in the bottom of the flow cross section at bed angles greater than the repose angle of the particles. The swarm of particles moved up and down repeatedly, decreasing in size until it finally disappeared upon reaching the minimum bed pressure drop. However, at bed angles lower than the repose angle of the particles, some particle dunes remained for a long time after the bed pressure drop reached its minimum. The bed pressure drop was no longer valid to indicate the relative bed inventory of solids and thus, a visual observation was used as an alternative to determine the emptying time. The gas velocity was the superficial velocity defined as the volumetric flow rate divided by the cross-sectional area of the vertical column. The particle diameter and density and the angle of the fluidized-bed relative to the horizontal plane were considered as experimental variables.

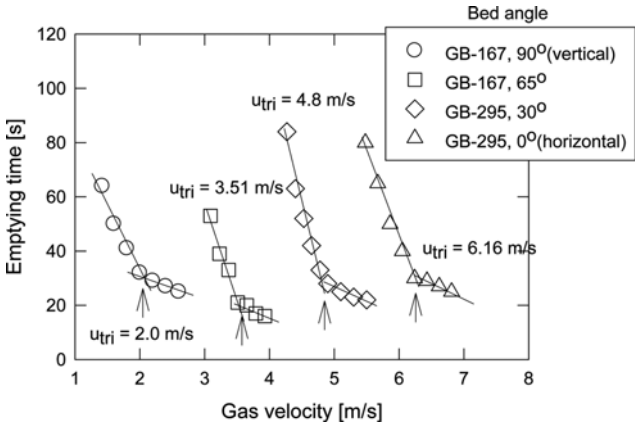

Fig. 2. Estimation of transport velocity of particles.

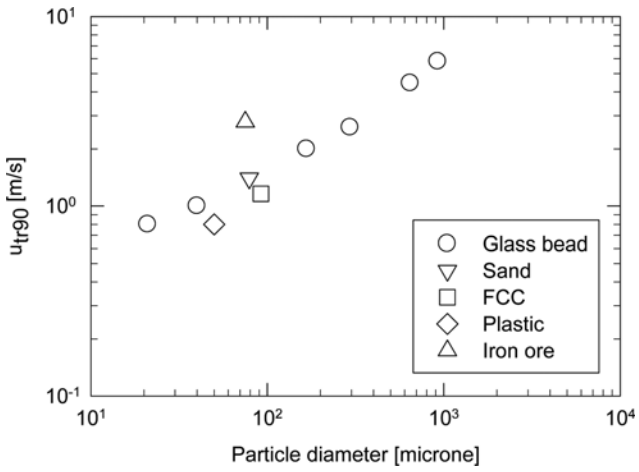

Fig. 3. Effect of particle diameter on transport velocity in vertical fluidized-beds.

RESULTS AND DISCUSSION

Fig. 2 shows the emptying times measured with variations of the particle size and angle of the fluidized-bed. Initially, the emptying time decreased rapidly, but gradually later on as the gas velocity, i.e., the drag force acting on the particles, increased. The transport velocity was then determined at the intersection of two straight lines fitting the steeply and the slowly decreasing trends, respectively [7].

Fig. 3 shows the transport velocity measured in the vertical fluidized-bed (u_{tr90}) in this study. u_{tr90} increased exponentially with particle size and density as usual [6,7,14,17] owing to an increase in the gravitational force acting on a single particle. Previous studies proposed relationships between the particle Reynolds number ($Re_{tr90}=d_p u_{tr90}\rho_g/\mu$) at u_{tr90} and the Archimedes number ($Ar=gd_p^3\rho_g(\rho_s-\rho_g)/\mu^2$), as listed in Table 2 [10,11,14,16,18,19]. However, the size of the fluidized-bed seemed to affect Re_{tr90} appreciably, and based on experimental data from present and previous studies [3-19], Re_{tr90} is written as:

$$Re_{tr90}=0.458Ar^{0.482}(H_f/d_t)^{0.357} \quad (2)$$

The regression coefficient (r^2) is 0.988. The exponent of Ar is very

Table 2. Existing correlations on transport velocity

Authors	Correlations	Applicable range
Lee and Kim [10]	$Re_{tr90}=2.91Ar^{0.354}$	$1.22\times10^2<Ar<5.7\times10^4$
Perales et al. [11]	$Re_{tr90}=1.41Ar^{0.483}$	$5\times10^2<Ar<2\times10^5$
Adanez et al. [14]	$Re_{tr90}=2.08Ar^{0.463}$	$4.5\times10^2<Ar<6.2\times10^4$
Smolders and Baeyens [16]	$Re_{tr90}=1.75Ar^{0.468}$	$1<Ar<10^5$
Bi and Fan [18]	$Re_{tr90}=2.28Ar^{0.419}$	$1.25\times10^2<Ar<1.45\times10^5$
Bi and Grace [19]	$Re_{tr90}=1.53Ar^{0.50}$	$2<Ar<4\times10^6$

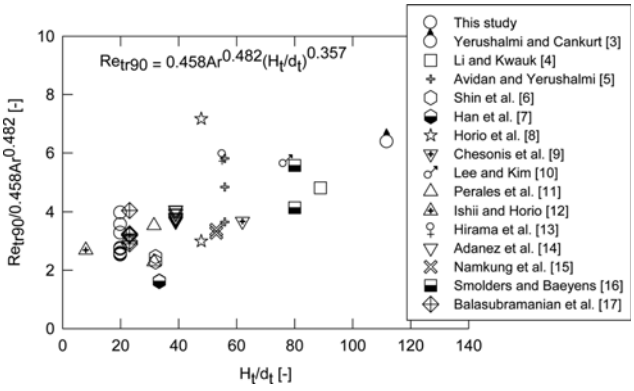

Fig. 4. Effect of aspect ratio of the fluidized-bed on Re_{tr90}.

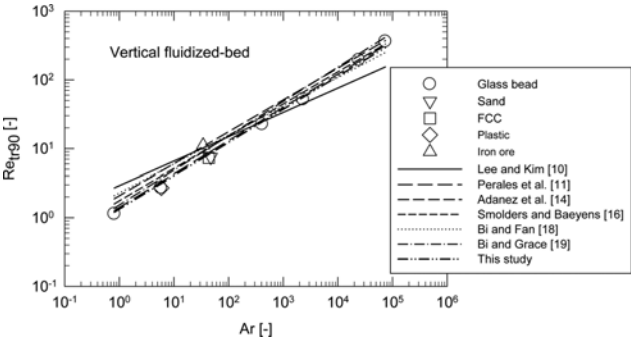

Fig. 5. Re_{tr90} versus Archimedes number.

similar to that of the correlation of Perales et al. [11]. Fig. 4 confirms that Re_{tr90} increases significantly with the aspect ratio of the fluidized-bed. To investigate the details of this effect, further experimental studies are needed in the future. Fig. 5 and Table 3 show a comparison between the correlations and u_{tr90} measured in this and previous studies [3-19]. The correlation in Eq. (2) agrees with the data from present and previous studies better than other correlations, based on the average relative deviation (ARD) calculated by Eq. (3).

$$\mathrm{ARD} = \frac{\sum_{i}^{N}\left(\frac{|\mathrm{Re}_{tr90,\,mea} - \mathrm{Re}_{tr90,\,cal}|}{\mathrm{Re}_{tr90,\,mea}}\right)_i}{\mathrm{N}} \quad (3)$$

Fig. 6 shows the transport velocity (u_{tri}) measured with variations of particle size and density at different angles of the fluidized-bed. u_{tri} increased as the bed angle relative to the horizontal plane decreased. This resulted from the decreasing vertical component of the gas velocity as the angle decreased. Appreciable increases appeared in u_{tri} of GB-21, GB-40, sand, and FCC particles as the bed angle decreased from 30° to 20°. The increase for GB-21 was certainly attributed to interparticle cohesive forces because of the mean particle diameter being smaller than the critical particle diameter [25], as shown in Table 1. A similar effect was somewhat suspected for GB-40, sand, and FCC particles, although the mean size of each particle group was greater than its own critical diameter. However, the effect was negligible for particles greater than 0.167 mm in size. During the transport of particles in this size range, an individual particle was observed rolling up the column wall in the bottom of

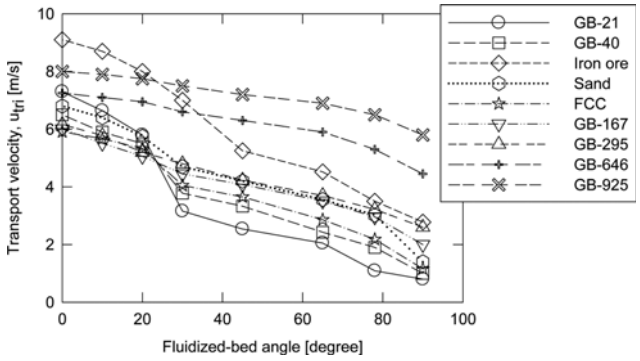

Fig. 6. Effects of particle property and angle of the fluidized-bed on transport velocity.

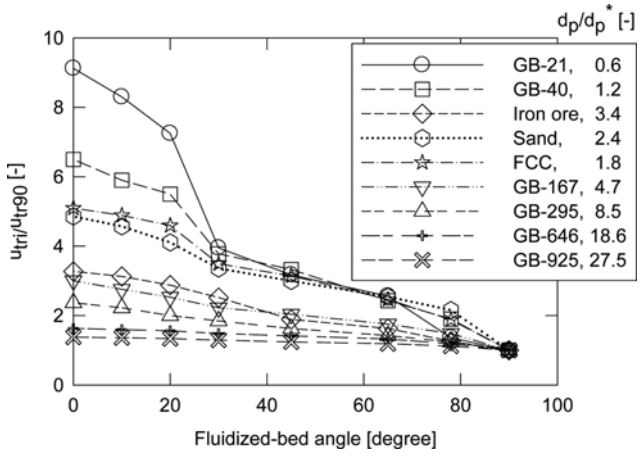

Fig. 7. Effects of particle diameter and angle of the fluidized-bed on u_{tri}/u_{tr90}.

the cross section without adhesion behavior even at a bed angle smaller than the repose angle of particles.

Fig. 7 shows the ratio of the transport velocity measured at an angle to that at 90°. It is convenient to discuss u_{tri} in a ratio form with u_{tr90} because u_{tri} originates in u_{tr90} and the correlation in Eq. (2) can give u_{tr90}. u_{tr90} measured in this study was used to set the ratio of u_{tri}/u_{tr90} to the same experimental standard. The ratio of u_{tri} to u_{tr90} seemed to decrease as either the angle of the fluidized-bed or the ratio of the particle diameter to the critical particle diameter increased. The decreasing slope of each particle group greater than 0.167 mm in mean diameter was fairly gradual for the present range of angles. The effect of the sum of the interparticle adhesion forces on u_{tri}/u_{tr90} appeared to be negligible for d_p/d_p^* ratios greater than 8.5 as the rolling effect governed particle transport at angles smaller than 30°. However, the decreasing slopes of GB-21, GB-40, sand, and FCC particles indicated three different trends according to the angular ranges. The transport velocity of the vertical bed (u_{tr90}) seemed to mainly affect u_{tri} for bed angles greater than the repose angle of particles (θ_r), and that of the horizontal bed (u_{tr0}) had the same effect for bed angles smaller than θ_r. There is a transition region in the trend of u_{tri} nearby the bed angle equal to θ_r. To describe the trend of u_{tri} with proper correlation, the angular effect was considered separately in two different ranges: from

Table 3. Comparison of utr90 between measured and calculated by correlations

Experimental data						u_{tr90} calculated by correlations						
Sources	Particle density [kg/m^3]	Particle diameter [μm]	Column diameter [m]	Column height [m]	Measured u_{tr90} [m/s]	Lee and Kim [10] [m/s]	Perales et al. [11] [m/s]	Adanez et al. [14] [m/s]	Smolders and Baeyens [16] [m/s]	Bi and Fan [18] [m/s]	Bi and Grace [19] [m/s]	This study [m/s]
This study												
GB-21	2364	21	0.05	1	0.80	1.90	0.90	1.32	1.11	1.47	0.97	0.85
GB-40	2440	40	0.05	1	1.00	1.99	1.21	1.72	1.47	1.75	1.36	1.15
Plastic	1272	50	0.05	1	0.80	1.60	0.98	1.39	1.18	1.41	1.09	0.93
Iron ore	4503	75	0.05	1	2.78	2.54	1.94	2.67	2.28	2.50	2.24	2.05
Sand	2591	79	0.05	1	1.40	2.13	1.70	2.31	1.99	2.14	1.97	1.60
FCC	1470	92	0.05	1	1.16	1.76	1.39	1.89	1.63	1.76	1.60	1.31
GB-167	2374	167	0.05	1	2.00	2.16	2.28	2.97	2.58	2.50	2.74	2.14
GB-295	2416	295	0.05	1	2.60	2.25	2.96	3.74	3.27	2.92	3.67	2.79
GB-646	2418	646	0.05	1	4.45	2.37	4.21	5.08	4.50	3.57	5.43	3.96
GB-925	2523	925	0.05	1	5.80	2.45	5.05	5.95	5.30	3.99	6.63	4.75
Yerushalmi and Cankurt [3]	2460	103	0.076	8.5	3.85	2.12	1.86	2.51	2.16	2.25	2.19	3.25
Li and Kwauk [4]	3160	54	0.09	8.0	2.45	2.23	1.57	2.19	1.87	2.11	1.79	2.53
Avidan and Yerushalmi [5]	1070	49	0.152	8.5	1.40	1.51	0.89	1.28	1.08	1.31	0.99	1.22
	1450	49	0.152	8.5	1.95	1.68	1.03	1.47	1.25	1.49	1.16	1.41
	1670	33	0.152	8.5	1.10	1.73	0.93	1.34	1.14	1.42	1.02	1.27
Shin et al. [6]	1720	205	0.078	2.5	1.58	1.95	2.14	2.77	2.41	2.31	2.58	2.38
	1720	395	0.078	2.5	2.28	2.03	2.87	3.58	3.14	2.73	3.58	3.19
Han et al. [7]	1400	1030	0.078	2.6	2.09	2.01	3.99	4.73	4.20	3.20	5.22	4.5
	1400	730	0.078	2.6	1.78	1.96	3.42	4.13	3.66	2.93	4.39	3.86
Horio et al. [8]	1000	60	0.05	2.39	0.92	1.49	0.95	1.34	1.14	1.34	1.06	1.22
	2600	106	0.05	2.39	4.50	2.17	1.94	2.60	2.24	2.31	2.28	2.50
Chesonis et al. [9]	3460	120	0.1	6.2	2.80	2.42	2.35	3.11	2.69	2.69	2.80	3.33
Lee and Kim [10]	2500	23	0.078	6.0	1.80	1.95	0.97	1.42	1.20	1.55	1.06	1.49
Perales et al. [11]	1715	80	0.092	2.9	1.60	1.84	1.40	1.92	1.65	1.81	1.61	1.56
	2650	212	0.092	2.9	1.98	2.28	2.67	3.43	2.99	2.79	3.26	2.96

Table 3. Continued

Experimental data					u_{tr90} calculated by correlations							
Sources	Particle density [kg/m^3]	Particle diameter [μm]	Column diameter [m]	Column height [m]	Measured u_{tr90} [m/s]	Lee and Kim [10] [m/s]	Perales et al. [11] [m/s]	Adanez et al. [14] [m/s]	Smolders and Baeyens [16] [m/s]	Bi and Fan [18] [m/s]	Bi and Grace [19] [m/s]	This study [m/s]
Ishii and Horio [12]	1780	61	0.2	1.6	1.10	1.83	1.26	1.76	1.50	1.71	1.43	0.86
Hirama et al. [13]	750	54	0.1	5.5	1.50	1.34	0.79	1.12	0.95	1.16	0.87	1.07
Adanez et al. [14]	1400	315	0.1	3.9	3.00	1.87	2.34	2.98	2.60	2.36	2.88	2.81
	1400	561	0.1	3.9	3.60	1.93	3.04	3.73	3.29	2.74	3.85	3.63
	1400	710	0.1	3.9	4.00	1.96	3.38	4.09	3.62	2.91	4.33	4.03
	1400	894	0.1	3.9	4.50	1.99	3.74	4.47	3.97	3.09	4.86	4.47
	2600	170	0.1	3.9	3.15	2.24	2.40	3.12	2.71	2.61	2.89	2.87
	2600	344	0.1	3.9	4.30	2.34	3.29	4.11	3.61	3.13	4.11	3.93
	2600	387	0.1	3.9	4.40	2.35	3.47	4.30	3.78	3.23	4.36	4.14
	2600	561	0.1	3.9	5.05	2.41	4.10	4.97	4.39	3.55	5.25	4.90
	2600	710	0.1	3.9	5.60	2.44	4.55	5.45	4.83	3.77	5.90	5.43
	2600	894	0.1	3.9	6.15	2.48	5.05	5.96	5.30	4.00	6.62	6.02
Namkung et al. [15]	1720	65	0.1	5.3	1.40	1.82	1.27	1.77	1.52	1.72	1.45	1.71
	3055	125	0.1	5.3	2.40	2.32	2.26	2.99	2.58	2.58	2.68	3.02
Smolders and Baeyens [16]	2700	70	0.1	8.0	2.20	2.14	1.64	2.25	1.93	2.11	1.89	2.55
	2600	90	0.1	8.0	3.25	2.15	1.80	2.44	2.10	2.22	2.10	2.80
Balasubramanian et al. [17]	2650	412	0.052	1.2	3.47	2.38	3.60	4.45	3.91	3.31	4.54	3.57
	2650	177	0.052	1.2	2.56	2.26	2.46	3.20	2.78	2.66	2.98	2.45
	1480	530	0.052	1.2	3.19	1.96	3.04	3.74	3.30	2.76	3.85	3.01
	1480	385	0.052	1.2	2.47	1.93	2.64	3.31	2.90	2.55	3.28	2.61
	676	385	0.052	1.2	1.86	1.46	1.80	2.30	2.01	1.83	2.21	1.79
	900	81	0.052	1.2	1.35	1.47	1.03	1.43	1.22	1.38	1.17	1.02
ARD by Eq. (3) for data of this study						0.57	0.16	0.46	0.29	0.43	0.30	0.13
ARD by Eq. (3) for previous data						0.30	0.27	0.28	0.25	0.25	0.29	0.21
ARD by Eq. (3) for all data						0.37	0.25	0.31	0.26	0.29	0.28	0.20

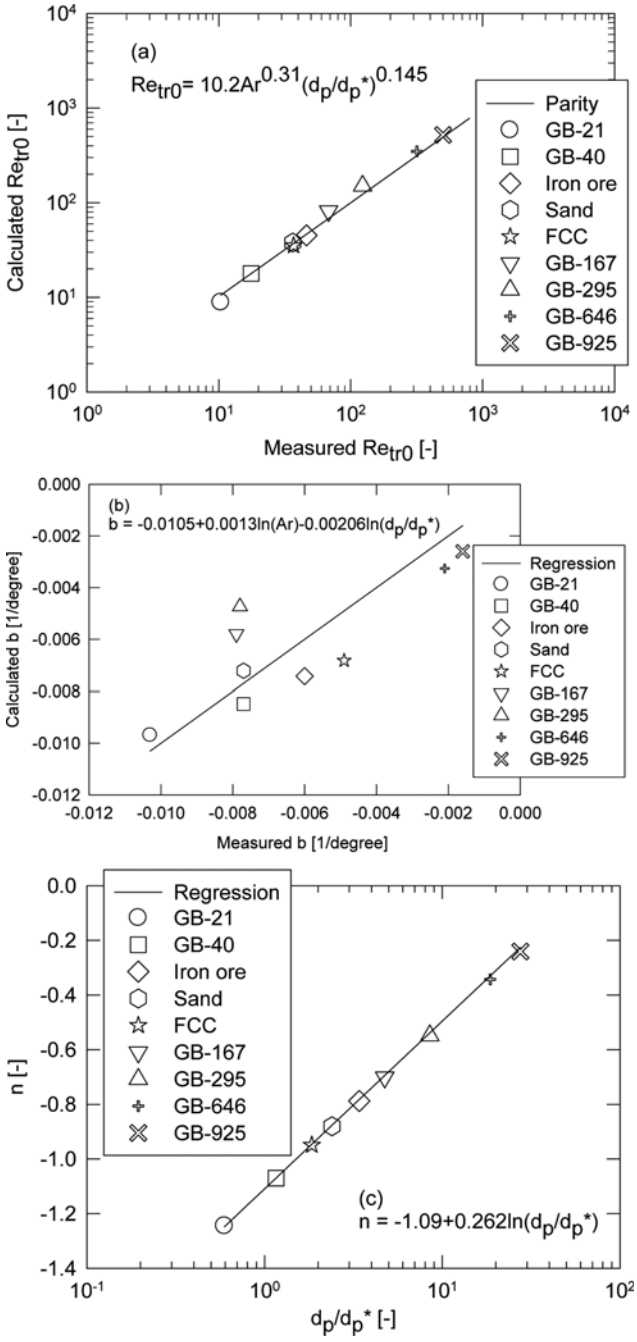

Fig. 8. Plots for correlations: (a) Eq. (4), (b) Eq. (6), and (c) Eq. (9).

zero to less than the repose angle (0°-20°) and from near the repose angle to 90° (30°-90°).

The transport velocity measured in the horizontal column is represented by the Reynolds number, Archimedes number, and a dimensionless particle diameter as (see Fig. 8(a)):

$$Re_{tr0}=10.2\ Ar^{0.310}\ (d_p/d_p^*)^{0.145} \quad (4)$$

The regression coefficient is 0.991. Similarly, the ratio u_{tri}/u_{tr0} or u_{tri}/u_{tr90} in each angular range is written as (Fig. 8(b), (c))

$$(u_{tri}/u_{tr0})=1+b\theta \qquad \text{for } 0^o<\theta\,[^o]<20^o \quad (5)$$

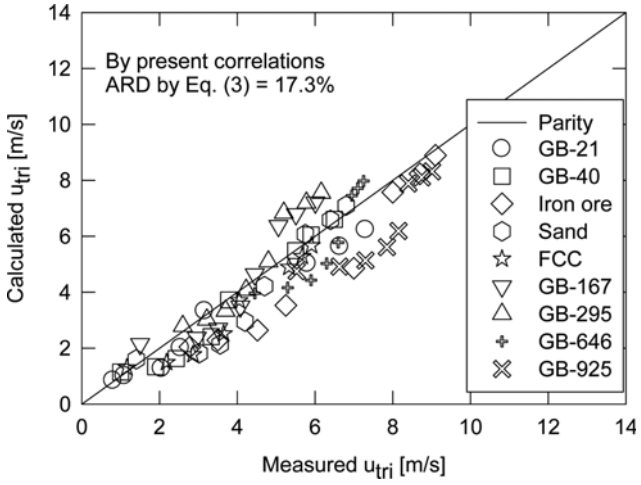

Fig. 9. Comparison of u_{tri} between measured and calculated by present correlations.

where

$$b=-0.0105+0.0013\ln(Ar)-0.00206\ln(d_p/d_p^*) \quad (6)$$

The regression coefficient is 0.737.

$$(u_{tri}/u_{tr90})=(\theta/90)^n \qquad \text{for } 30^o<\theta\,[^o]<90^o \quad (8)$$

where

$$n=-1.09+0.262\ln(d_p/d_p^*) \quad (9)$$

The regression coefficient is 0.994. The u_{tri} between 20° and 30° is determined proportionally by interpolation between u_{tr20} and u_{tr30}. To predict u_{tri}, Eqs. (4) to (6) are recommended for bed angles between 0° and θ_r-5^o, Eqs. (2), (8), and (9) are recommended for bed angles between θ_r+5^o and 90°, and linear interpolation is recommended between u_{tri}s at θ_r-5^o and θ_r+5^o for bed angles between θ_r-5^o and θ_r+5^o.

Fig. 9 shows the comparison between the measured and the calculated transport velocities. The present correlations agreed with the measured data within an average relative error of 17.3%. However, the application of the present correlations is limited to the following ranges: $21<d_p$ [μm]<925, $1{,}470<\rho_s$ [kg/m^3]$<4{,}503$, $0.6<d_p/d_p^*$ [-]<27.5, $0.05<d_t$ [m]<0.2, $1<H_t$ [m]<8.5, $8<H_t/d_t$ [-]<112, and $0^o<\theta\,[^o]<90^o$. To investigate effects of other variables relating to gas properties such as the gas density and viscosity, further studies will be needed in the future.

CONCLUSIONS

The transport velocity in an inclined fluidized-bed was investigated by varying the particle diameter and density and the bed angle relative to the horizontal plane, and the following conclusions were derived. The transport velocity for the vertical fluidized-bed (u_{tr90}) was found to increase significantly with the aspect ratio of the fluidized-bed. The transport velocity (u_{tri}) decreased as the angle of the fluidized-bed increased. The ratio of the transport velocity to the transport velocity of the vertical fluidized-bed (u_{tri}/u_{tr90}) also decreased as either the angle of the fluidized-bed or the ratio of

particle diameter (d_p) to critical particle diameter (d_p^*) increased. Correlations for the transport velocity according to the bed angle relative to the horizontal plane were proposed successfully, based on the experimental data.

ACKNOWLEDGEMENTS

This work was supported by the Energy Efficiency & Resources Core Technology Program of the Korea Institute of Energy Technology Evaluation and Planning (KETEP), granted financial resource from the Ministry of Trade, Industry & Energy, Republic of Korea (2011201020004B, 20142010201830).

NOMENCLATURE

Ar : Archimedes number, $\rho_g d_p^3(\rho_s-\rho_g)g/\mu^2$ [-]
b : constant [1/degree]
d_p : specific surface mean particle diameter [m]
d_p^* : critical particle diameter, i.e. the maximum particle diameter at which the sum of interparticle adhesion forces influence dominantly in particle entrainment [m]
d_t : column diameter [m]
g : gravitational acceleration, 9.8 [m/s^2]
H_t : column height [m]
N : number of data [-]
n : exponent [-]
Re_{tr0} : Reynolds number for u_{tr0}, $d_p u_{tr0}\rho_g/\mu$ [-]
Re_{tr90} : Reynolds number for u_{tr90}, $d_p u_{tr90}\rho_g/\mu$ [-]
u_{tr90} : transport velocity for the vertical fluidized-bed [m/s]
u_{tr0} : transport velocity for the horizontal bed [m/s]
u_{tri} : transport velocity for the fluidized-bed inclined to the horizontal plane with angle i in degree [m/s]

Greeks

θ : angle of the fluidized-bed inclined to the horizontal plane [degree]
θ_r : repose angle of particles [degree]
μ : gas viscosity [Pa s]
ρ_g : gas density [kg/m^3]
ρ_s : particle density [kg/m^3]

Subscripts

cal : calculated
mea : measured

REFERENCES

1. P. S. Youn and J.-H. Choi, *Korean Chem. Eng. Res.*, **52**, 81 (2014).
2. D. Kunii and O. Levenspiel, *Fluidization engineering*, 2nd Ed., Butterworth-Heinemann, Boston (1991).
3. J. Yerushalmi and N. T. Cankurt, *Powder Technol.*, **24**, 187 (1979).
4. Y. Li and M. Kwauk, in *Fluidization*, J. R. Grace and J. M. Matsen Eds., Plenum Press, New York, 537 (1980).
5. A. A. Avidan and J. Yerushalmi, *Powder Technol.*, **32**, 223 (1982).
6. B. C. Shin, Y. B. Koh and S. D. Kim, *Korean Chem. Eng. Res.*, **20**, 253 (1984).
7. G. Y. Han, G. S. Lee and S. D. Kim, *Korean J. Chem. Eng.*, **2**, 141 (1985).
8. M. Horio, H. Ishii and M. Nishimuro, *Powder Technol.*, **70,** 229 (1992).
9. D. C. Chesonis, G. E. Klinzing, Y. T. Shaah and C. G. Dassori, *Ind. Eng. Chem. Res.*, **29**, 1792 (1990).
10. G. S. Lee and S. D. Kim, *Powder Technol.*, **62**, 207 (1990).
11. J. F. Perales, T. Coll, M. F. Llop, L. Puigjaner, J. Arnaldos and J. Casal, in *Circulating Fluidized Bed Technology III*, P. Basu, M. Horio and M. Hasatani Eds., Pergamon Press, New York, 73 (1991).
12. H. Ishii and M. Horio, *Adv. Powder Technol.*, **2**, 25 (1991).
13. T. Hirama, H. Takeuchi and T. Chiba, *Powder Technol.*, **70**, 215 (1992).
14. J. Adanez, L. F. de Diego and P. Gayan, *Powder Technol.*, **77**, 61 (1993).
15. W. Namkung, S. W. Kim and S. D. Kim, *Chem. Eng. J.*, **72**, 245 (1999).
16. K. Smolders and J. Baeyens, *Powder Technol.*, **119**, 269 (2001).
17. N. Balasubramanian, C. Srinivasakannan and C. A. Basha, *Adv. Powder. Technol.*, **16**, 247 (2005).
18. H. T. Bi and L. S. Fan, *AIChE J.*, **38**, 297 (1992).
19. H. T. Bi and J. R. Grace, *Int. J. Multiphase Flow*, **21**, 1229 (1995).
20. B. Du, W. Warsito and L. S. Fan, *Ind. Eng. Chem. Res.*, **45**, 5384 (2006).
21. D. Geldart, *Powder Technol.*, **7**, 285 (1973).
22. W. C. Yang, in *Handbook of Fluidization and Fluid-Particle Systems*, W. C. Yang Eds., Marcel Dekker, New York, Chapter 1, 26 (2003).
23. S. H. Kang, Powder Technology, Hee Joong Dang, Seoul, Korea, 122 (1995).
24. A. Haider and O. Levenspiel, *Powder Technol.*, **58**, 63 (1989).
25. X. X. Ma and K. Kato, *Powder Technol.*, **95**, 93 (1998).
26. J. Li and K. Kato, *Powder Technol.*, **118**, 209 (2001).